Design and commissioning of resistive foil bolometer diagnostics on the ST40 tokamak

D. M. Harryman,[1] C. Colgan,[1] J. Lovell,[2] M. Moscheni,[1] G. Naylor,[1] A. Rengle,[1] M. Sertoli,[1] A. Sladkomedova,[1] and R. Thwaites[1]

[1)]*Tokamak Energy Ltd, Abingdon, OX14 4SD, UK*

[2)]*Oak Ridge National Laboratory, Oak Ridge, TN 37831, USA*

(*Electronic mail: daniel.harryman@tokamakenergy.com)

(Dated: 22 July 2024)

Following successful campaigns on the compact high field spherical tokamak ST40, resistive gold foil bolometers have now been installed to measure the radiated power profile. Positioned on the midplane, two bolometer cameras offer perspectives of the horizontal and vertical planes, while the third camera, situated above the midplane, provides a vertical view of the top divertor plates including the X-point and the strike points. These cameras use a commercial off-the-shelf data acquisition platform with modules specifically designed for bolometers in a Wheatstone bridge configuration, providing both phase sensitive detection and in-situ calibration. This paper presents an overview of the design and functionality of all three cameras, and the commissioning of the horizontal plane camera. The commissioning of the horizontal camera shows data from a range of plasma pulses, presenting positive correlation between the relative profiles measured from the bolometer camera and an absolute extreme ultraviolet diode camera viewing along similar lines of sight.

I. INTRODUCTION

Resistive foil bolometers have been deployed in various magnetic confinement facilities for measuring the radiated power profile from a plasma[1–3]. Measurements of radiated power are important when attempting to understand the loss mechanisms taking place in the plasma. Typically, foil bolometers employ gold or platinum foils connected to thermistors in a Wheatstone bridge configuration[4]. Each sensor unit deployed on ST40 is comprised of eight gold foils each 5 µm thick. On the underside of each foil is a pair of gold meander resistors used as thermistors. Four of the foils are exposed to the plasma and used for measurement, the other four are used for background reference. Each exposed and reference foil is used in a pair to form a Wheatstone bridge with the meander resistors. In total four Wheatstone bridges are in each sensor unit yielding four measurement channels[4]. A comprehensive understanding and discussion of these sensors can be found in references[3–5].

Until recently, bolometer diagnostics had not been installed on the ST40 spherical tokamak, which is owned and operated by Tokamak Energy Ltd[6]. Three cameras featuring 5 µm thick gold foil bolometer sensors have now been deployed on to ST40. Two cameras are situated on the midplane, providing vertical and horizontal views of the RZ poloidal plane and XY toroidal plane respectively, while a third camera offers vertical views of the top divertor plates. This paper discusses the design of each camera, with a focus on data from the first camera installed, the XY horizontal camera, which is explored to validate and commission the diagnostic design.

A. Theory

When energy is deposited on each bolometer foil, the temperature of the foil increases. Thermistors are connected to the foils, resulting in a resistance that changes with the foil temperature. By integrating the foils into a pinhole camera each foil is restricted to a specific view of the plasma. Each foil is composed of 5 µm thick gold making the spectral response of the detector determined by the photon absorption characteristics of the gold foil. Specifically, the 5 µm thick gold foils absorb photons in the range 2.5 eV to 10 keV, exhibiting a non-flat response in the range between approximately 2.5 eV and 100 eV. Further details regarding the spectral response of gold foils can be found in references[3,7]. The impurity content in ST40 is expected to be mainly C from the outer walls and Ar from gas puffing. The vacuum chamber is manufactured from stainless steel leading to impurities of Ni, Fe, and Cr with additional Mo being contributed from the divertor tiles. Preliminary analysis has shown that the Ar and C will dominate the radiated power emission, with emission that is absorptive for the gold foils.

To obtain a measurement from the bolometer, the Wheatstone bridge is excited with an AC voltage. Voltage is measured at the central points of the Wheatstone bridge indicating the difference between each side of the bridge caused by the increasing temperature of the exposed foils. The incident power on the bolometer foil is calculated using the equation:

$$P = \frac{1}{S}\left(A + \tau\frac{\mathrm{d}A}{\mathrm{d}t}\right) \tag{1}$$

Where P represents the power, A is the measured signal amplitude from the bridge in volts, t is time, τ is the cooling time response of the bolometer, and S denotes the V/W sensitivity of the bolometer[1,8]. The sensitivity and cooling time of the foil are determined during an in-situ calibration routine conducted on the bolometers. This calibration involves DC ohmic heating of the foils with a known amount of power in addition to the AC excitation voltage to measure the sensitivity. After heating is discontinued, the foils begin to cool, allowing for the measurement of the cooling time response[1].

II. SYSTEM DESIGN

Three bolometer cameras have now been installed onto ST40: a vertical RZ camera with twelve Lines Of Sight (LOS), a horizontal XY camera with eight LOS, and a vertical divertor camera, also with eight LOS. These cameras contain bolometer sensor units within 316 stainless steel housing, each with a rectangular pinhole at the front. Figure 1 provides a sectional view of the vertical RZ camera, showcasing the bolometers arranged in an arc configuration. Custom connectors manufactured from PolyEther Ether Ketone (PEEK) are affixed to the back for electrical connection. To stop reflections inside the cameras the internal surfaces have been coated with colloidal graphite. Additionally the pinhole which is machined from 1 mm thick tungsten has knife edges around the pinhole to mitigate reflections from the pinhole edge reaching the sensor. The pinhole dimensions are between 3 and 6 mm depending on the camera. The etendue of each channel of the installed XY camera are between 1.6×10^{-8} and $1.8 \times 10^{-8} \mathrm{m}^2\,\mathrm{sr}$ depending on the channel.

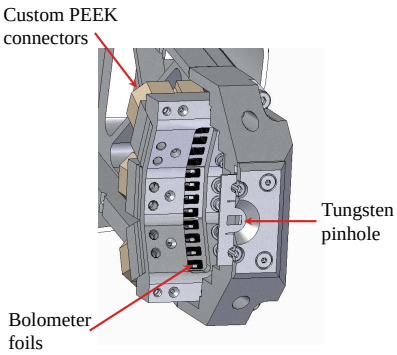

FIG. 1. Annotated CAD of vertical RZ bolometer camera (section view)

A. Lines of Sight

The LOS of each camera have been mapped out using an in-house ray tracing framework. This framework allows for the simulation of LOS and calculation of pinhole sizes. This generates plots featuring the central line through the LOS, along with two projections from the sensor: one through a point pinhole and the other accounting for the real pinhole dimensions. These projections are differentiated with varying shading. Figure 2 illustrates the LOS of the XY camera, with the impact parameter marked on each LOS. The impact parameter in this context is the minimal R value that the centre of each LOS crosses.

Figure 3 shows the LOS of the vertical RZ camera. This camera offers a near continuous radial view of the entire plasma. Both the XY and RZ cameras are installed on midplane ports and offer full plasma view across their respective plane.

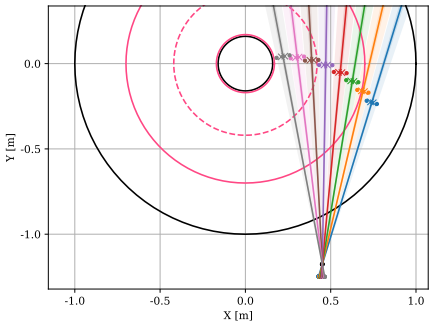

FIG. 2. XY view of simulated LOS for the XY bolometer camera mapped onto ST40.

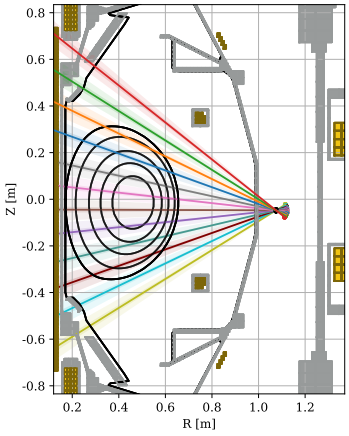

FIG. 3. RZ view of simulated LOS for the radial RZ bolometer camera mapped onto ST40.

A third bolometer camera has been developed to increase the suite of divertor diagnostics on ST40. This camera has been installed after successfully achieving diverted plasma in the last ST40 physics campaign[9]. This camera is designed to provide views of the top inner and outer divertor plates and the X point (see Fig 4).

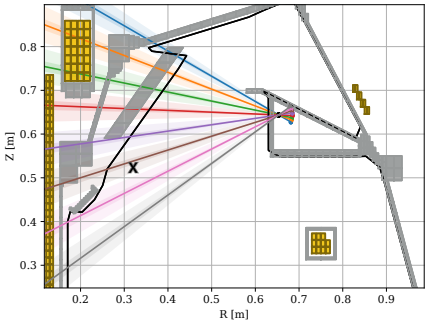

FIG. 4. RZ view of simulated LOS for the top divertor bolometer camera mapped onto ST40. Approximate X-point location for ST40 diverted plasma pulses has been included.

A spatial calibration for each camera was performed in the lab after assembly. Given the reflectivity of gold[3], a 400 nm laser was used for this process. The camera was mounted onto an optical turntable centered on the pinhole, with the laser shining at the pinhole. The spatial calibration was obtained by rotating the turntable and capturing the bolometer response. The spatial calibration aligned well with the design values, with a typical error of 1-3%. Currently, the viewing cones of the camera are mapped onto the vessel using a Computer Aided Design (CAD) model, and discussions to perform in-situ spatial mapping are ongoing.

B. Electronics and Software

All bolometers used on ST40 are connected to a single ACQ2106 unit manufactured by D-TACQ. The ACQ2106 unit is equipped with four BOLO8 modules, with each module providing functionality for two bolometer sensor units[10]. Each bolometer sensor unit is connected to a vacuum feedthrough flange via eight shielded twisted pair cables. Bolometers may be limited by the noise picked up in the systems[11], where one potential source of noise pickup is from the in-vessel cables. Care has been taken in the design of the cameras to keep the length of in-vessel cables as short as possible, with lengths between 15 and 30 cm for the different cameras. On the air side a separate cable with individually shielded twisted pairs is used for each sensor unit routing back to the ACQ2106.

The selection of the ACQ2106 and BOLO8 cards was based on their established performance at other tokamak facilities[1,2]. The BOLO8 modules are specifically designed for these types of sensors where they provide AC excitation voltages of ± 10 V, lock-in detection measurements, and in-situ calibration[10]. The BOLO8 samples at a rate 1 MS/s where the onboard processing providing the lock-in detection decimates the data by a factor of 100 yielding an effective sample rate of 10 kS/s.

The ACQ2106 unit runs an embedded Linux Operating System (OS), in-house software packages have been developed to run on the OS for communicating with the ST40 pulse coordination control system. The system is configured to conduct an in-situ calibration of all bolometer sensors before each plasma pulse. Subsequently, data from the ACQ2106 is directly saved to an MDS+ database following each pulse. The saved data includes the amplitude and phase measured during the pulse, as well as traces obtained from the in-situ calibration routine. During post-processing, the calibration routine data is analysed to compute the sensitivity and cooling time and used with Eq 1 to obtain the power measurements.

III. COMMISSIONING

In the most recent ST40 campaign, only the XY horizontal bolometer camera was installed. This paper explores commissioning data obtained from this campaign and camera. To ensure commissioning of the camera, the collected data was compared with data from other diagnostics, including a fast visible light camera, Thomson Scattering (TS) system, and an unfiltered Absolute eXtreme UltraViolet (AXUV) diode camera[12].

The AXUV diode camera is installed on the same midplane port as the bolometer camera and has similar LOS views. This camera features an AXUV16ELG sensor, providing sixteen LOS. The AXUV diode camera has two AXUV16ELG sensors, one unfiltered and one filtered with 25 µm beryllium film. All the AXUV data presented in this paper is obtained from the unfiltered diode as its wider sensitivity range is closer aligned with that of the bolometers[2]. The time response of the AXUV diodes is much faster than the bolometers, and as such the AXUV diode camera has a wider temporal bandwidth that should be considered when comparing the systems[2].

In order to represent the respective channel by channel crossover between the bolometer and AXUV cameras Fig 5 is presented. These figures show the RZ mapping from both cameras at the impact parameter of each LOS demonstrating that there exists a significant overlap. Seen in Fig 5 the innermost LOS on the AXUV camera, LOS 1, is partially blocked by the central column, as such this channel has been omitted from the brightness profiles in this paper.

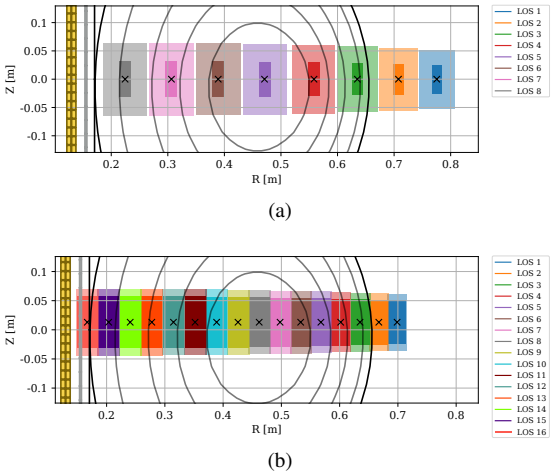

FIG. 5. RZ view of simulated LOS for the horizontal XY cameras at the impact parameter of each LOS. The solid regions represent the point projection of each LOS whereas the shaded region accounts for the pinhole size. (a) Bolometer camera, (b) AXUV camera.

A. Results

Figure 6 presents images captured by a visible camera during ST40 plasma pulse 11315. This pulse showcases a limited plasma scenario where an Internal Reconnection Event (IRE)[13] occurs around 135 ms. Figure 7 displays the power and voltage measurements from each XY bolometer and AXUV diode channel for the same plasma pulse. Both datasets in Figure 7 have been filtered into 1 ms bins to minimise differences in time response between the two systems. Minimal signal is observed on the bolometer channel LOS 1,

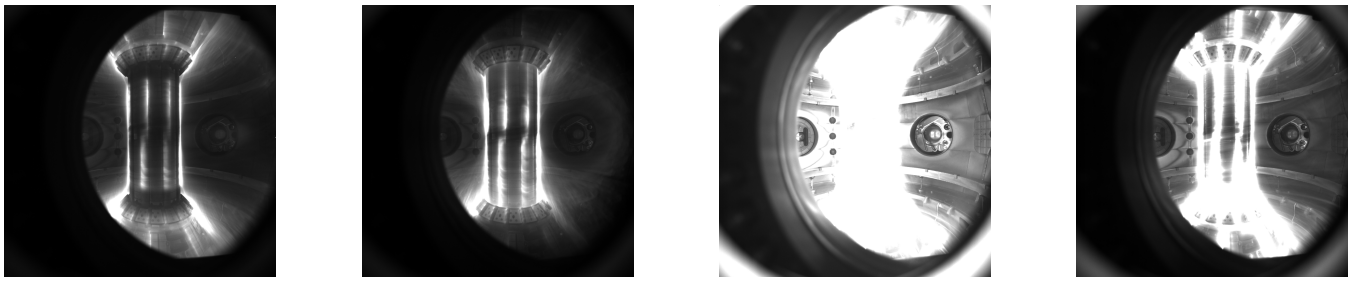

(a) (b) (c) (d)

FIG. 6. Fast visible camera images from ST40 plasma pulse 11315. (a) 80 ms, (b) 134.5 ms, (c) 134.7 ms, (d) 134.9 ms.

allowing this channel to serve as a reference for noise level assessment. The standard deviation of the bolometer LOS 1 signal depicted in Fig 7 is approximately 40 µW. Examining the same signal without 1 ms binning gives a standard deviation between 160 and 200 µW. Examining Fig 7 both systems display similar shapes and features, including a local maximum at 80 ms and a spike at 135 ms. The spike at 135 ms is the response to the IRE, the synchronised response observed in both the visible camera images (see Fig 6) and the raw traces (see Fig 7) confirms the time synchronization between the three cameras.

Figure 8 displays data from the same pulse as Fig 7, where profiles have been extracted from both XY cameras at 80 ms. The profiles provided have been calculated, taking into account the etendue of each LOS, and presented against the respective impact parameter. The values in Fig 8 represent the mean brightness measured over the specified time range with standard deviation as the error. Also marked in Fig 8 is the magnetic axis of the plasma R_{mag} and the Last Closed Flux Surface (LCFS) both calculated from equilibrium fitting. The relative shape of the AXUV and bolometer profiles remains similar in the 80 ± 2 ms profiles, with a peak occurring in both when R is approximately 0.5 m, closely aligning with R_{mag}.

ST40 has recently undergone commissioning to operate diverted plasma configurations[9]. Figure 9 demonstrates the bolometer and AXUV camera responses to both a limited and diverted plasma configuration. Two pulses are examined for comparison, 11317 as a limited pulse, and 11522 as a diverted pulse. For both pulses beam heating is applied from both Heating Neutral Beam Injectors (HNBI) and RFX, where the HNBI applies 1 MW of heating power and the RFX applies 0.5 MW. In the limited pulse both the HNBI and RFX are applied for approximately 90 ms, whereas for the diverted pulse the RFX is applied for 90 ms and the HNBI for 180 ms.

The radiated power profile is in part formed of the electron density and temperature profile, these profiles measured by the TS are presented in Fig 10 for the same time period and plasma pulses as Fig 9. The electron density profile is flatter and broader for the diverted plasma with the temperature profile shifted further outboard. This matches the diverted brightness profiles with both shifted further outboard with a flatter shape. Examining the TS profiles for the limited plasma a peak in the electron density profile measured at 0.5 m corresponding with the peak measured in Fig 9.

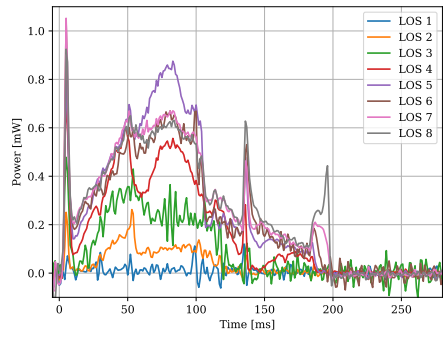

(a)

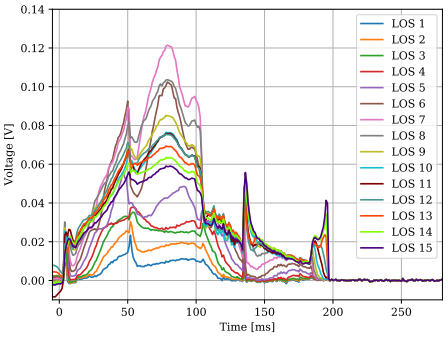

(b)

FIG. 7. Signals measured from horizontal XY cameras for ST40 plasma pulse 11315 filtered into 1 ms bins. Each LOS follows the same colour mapping as the channels in Fig 5. (a) Bolometer camera, (b) AXUV camera.

The relative profile shapes measured between the bolometer and AXUV cameras exhibit broad similarity. Some difference in relative profiles is expected given the difference in spectral response between the cameras, this gives confidence in the proper functionality of both camera systems. This paper has presented a qualitative agreement between both cameras in measuring the profile of radiated power. Furthermore additional checks have been performed using the TS system and

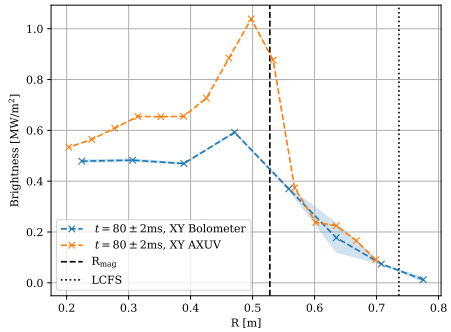

FIG. 8. Profiles taken from ST40 plasma pulse 11315. The R value is given as the LOS impact parameter, the brightness is the mean measured over the time range and the error the standard deviation.

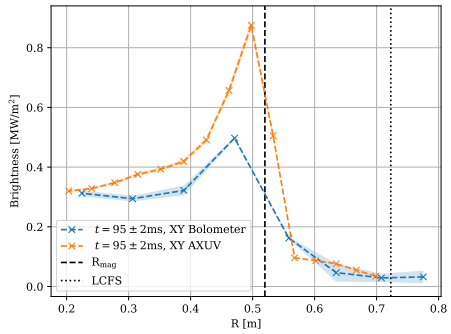

(a)

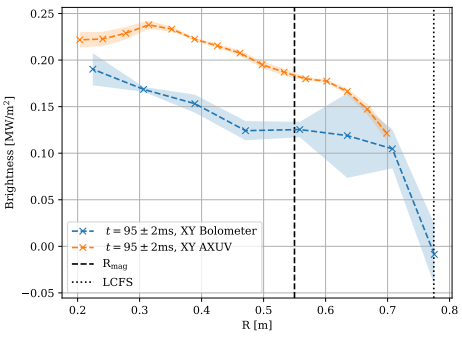

(b)

FIG. 9. Bolometer and AXUV brightness profiles. The R value is given as the LOS impact parameter, the brightness is the mean measured over the time range and the error the standard deviation. (a) Limited plasma pulse 11317, (b) Diverted plasma pulse 11522.

a visible light camera with correlation between all systems. There exists a discrepancy in the absolute brightness values measured between the two XY cameras. Currently, it remains unclear whether this discrepancy is from the spectral response of the different detectors, the temporal bandwidth of the instruments, or if it is an artifact resulting from the analysis.

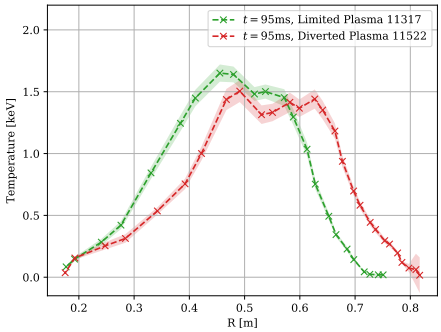

(a)

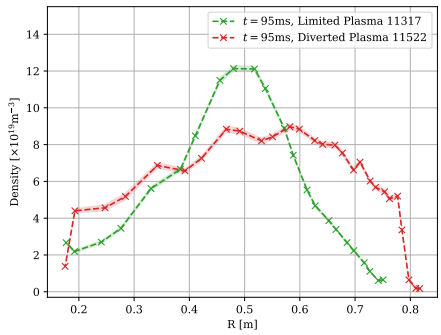

(b)

FIG. 10. TS profiles taken for diverted plasma pulse 11522 and limited pulse 11317. (a) Electron temperature profiles, (b) Electron density profiles.

Another theory is that with detailed error propagation analysis the two systems may be correlated better than they currently appear. Importantly, this discrepancy does not imply that the diagnostic system is non-functional; rather, it underscores the need for further investigation to comprehend the differences between the two cameras.

IV. CONCLUSION

In summary, the first bolometer diagnostic system for ST40 has been successfully installed and commissioned. This achievement bodes well for the deployment and data collection of the new systems based on a similar design. With the design now validated in-depth analysis and interpretation to understand the data measured by the diagnostic can commence.

Future planned measurement studies and analysis will be performed to attempt to identify the difference in absolute measurements. Additionally, once data becomes available from the bolometer RZ camera (see Fig 3), it will be compared with an equivalent AXUV RZ camera also recently installed on ST40. Other studies are also planned comparing data between the divertor bolometer camera with erosion spectroscopy diagnostics and an infrared camera.

ACKNOWLEDGMENTS

This work was supported in part by the U.S. Department of Energy under Award DE-AC05-00OR22725.

[1]J. Lovell, G. Naylor, A. Field, P. Drewelow, and R. Sharples, "An fpga-based bolometer for the mast-u super-x divertor," Review of Scientific Instruments **87** (2016), 10.1063/1.4961556.

[2]U. A. Sheikh, L. Simons, B. P. Duval, O. Février, D. Moret, A. Allegrucci, M. Bernert, F. Crisinel, T. Tersztyánszky, and O. Villinger, "Radcam—a radiation camera system combining foil bolometers, axuv diodes, and filtered soft x-ray diodes," Review of Scientific Instruments **93** (2022), 10.1063/5.0095907.

[3]A. Huber, K. McCormick, P. Andrew, P. Beaumont, S. Dalley, J. Fink, J. Fuchs, K. Fullard, W. Fundamenski, L. Ingesson, *et al.*, "Upgraded bolometer system on jet for improved radiation measurements," Fusion Engineering and Design **82**, 1327–1334 (2007), proceedings of the 24th Symposium on Fusion Technology.

[4]K. F. Mast, J. C. Vallet, C. Andelfinger, P. Betzler, H. Kraus, and G. Schramm, "A low noise highly integrated bolometer array for absolute measurement of vuv and soft x radiation," Review of Scientific Instruments **62**, 744–750 (1991).

[5]S. Jahanbakhsh, J. D. Hare, H. Meister, C. Ingesson, M. Majewski, F. Penzel, S. Schmitt, U. Walach, and M. Dubois, "Calibration and thermal test results of prototype bolometer sensors for iter fusion reactor," Review of Scientific Instruments **94** (2023), 10.1063/5.0134449.

[6]S. McNamara, O. Asunta, J. Bland, P. Buxton, C. Colgan, A. Dnestrovskii, M. Gemmell, M. Gryaznevich, D. Hoffman, F. Janky, *et al.*, "Achievement of ion temperatures in excess of 100 million degrees kelvin in the compact high-field spherical tokamak st40," Nuclear Fusion **63**, 054002 (2023).

[7]U. A. Sheikh, B. P. Duval, B. Labit, and F. Nespoli, "A novel carbon coating technique for foil bolometers," Review of Scientific Instruments **87** (2016), 10.1063/1.4961271.

[8]L. Giannone, K. Mast, and M. Schubert, "Derivation of bolometer equations relevant to operation in fusion experiments," Review of Scientific Instruments **73**, 3205–3214 (2002).

[9]S. A. M. McNamara, A. Alieva, M. S. Anastopoulos Tzanis, O. Asunta, D. Battaglia, N. Bertelli, J. Bland, H. Bohlin, P. J. Bonofiglo, *et al.*, "Overview of high temperature plasmas in the ST40 compact high-field spherical tokamak [manuscript submitted for publication]," (2024).

[10]D-Tacq Solutions, "BOLO8BLF product specification," (2023), rev 3.

[11]J. Lovell, M. L. Reinke, A. R. Field, and B. A. Lomanowski, "Overview and first measurements of the mast upgrade bolometer diagnostic," Review of Scientific Instruments **94** (2023), 10.1063/5.0128750.

[12]C. Colgan, H. Bohlin, P. F. Buxton, D. M. Harryman, O. Jones, H. F. Lowe, G. Naylor, T. O'Gorman, T. Pyragius, M. Sertoli, A. Sladkomedova, S. Sundaresan, and R. Thwaites, "Soft X-ray tomography on the high field spherical tokamak ST40 [manuscript submitted for publication]," (2024).

[13]S. Kim, J. Y. Jang, Y. Kim, and Y. Hwang, "Acceleration of ion rotation during internal reconnection events in the versatile experiment spherical torus (vest)," Nuclear Fusion **61**, 126011 (2021).